energies

MDPI

Article

Implications of Cation Interdiffusion between Double Perovskite Cathode and Proton-Conducting Electrolyte for Performance of Solid Oxide Fuel Cells

Nadezhda S. Tsvetkova [1,*], Dmitry A. Malyshkin [2], Ivan L. Ivanov [2], Dmitry S. Tsvetkov [1,2] and Andrey Yu. Zuev [1,*]

[1] Institute of Natural Sciences and Mathematics, Ural Federal University, 19 Mira St., 620002 Ekaterinburg, Russia
[2] Laboratory of Hydrogen Energy, Ural Federal University, 19 Mira St., 620002 Ekaterinburg, Russia
* Correspondence: nadezhda.tcvetkova@urfu.ru (N.S.T.); andrey.zuev@urfu.ru (A.Y.Z.)

Abstract: Chemical compatibility and cation interdiffusion between the double perovskite cobaltites RBaCo$_2$O$_{6-\delta}$ (R = Gd, Pr) and proton-conducting electrolyte BaZr$_{0.8}$Y$_{0.2}$O$_{3-\delta}$ were studied. Chemical interaction was found to occur already at 1100 °C as a result of the partial dissolution of RBaCo$_2$O$_{6-\delta}$ (R = Gd, Pr) in BaZr$_{0.8}$Y$_{0.2}$O$_{3-\delta}$. Analysis of the element distribution along the cross sections of diffusion couples RBaCo$_2$O$_{6-\delta}$(R = Gd, Pr) | BaZr$_{0.8}$Y$_{0.2}$O$_{3-\delta}$ showed strong interdiffusion of cations, with cobalt being the most mobile one. Its diffusion depth in the electrolyte reaches up to several hundreds of micrometers. The addition of NiO as a sintering aid to BaZr$_{0.8}$Y$_{0.2}$O$_{3-\delta}$ promotes cation diffusion especially through the grain boundary mechanism, increasing the diffusion depth of Co. The possible implications of cation interdiffusion on the performance of proton-conducting SOFCs are discussed based on the results obtained.

Keywords: solid oxide fuel cells; cation interdiffusion; double perovskites; cathode materials; proton-conducting solid electrolyte

check for updates

Citation: Tsvetkova, N.S.; Malyshkin, D.A.; Ivanov, I.L.; Tsvetkov, D.S.; Zuev, A.Y. Implications of Cation Interdiffusion between Double Perovskite Cathode and Proton-Conducting Electrolyte for Performance of Solid Oxide Fuel Cells. *Energies* **2023**, *16*, 2980. https://doi.org/10.3390/en16072980

Academic Editor: Vladislav A. Sadykov

Received: 1 February 2023
Revised: 10 March 2023
Accepted: 22 March 2023
Published: 24 March 2023

Copyright: © 2023 by the authors. Licensee MDPI, Basel, Switzerland. This article is an open access article distributed under the terms and conditions of the Creative Commons Attribution (CC BY) license (https://creativecommons.org/licenses/by/4.0/).

1. Introduction

Solid oxide fuel cells (SOFCs) are solid-state electrochemical devices that convert the chemical energy of the fuel (hydrogen, natural gas and other hydrocarbons) directly into electrical energy and possess high energy conversion efficiency and low environmental impact [1–3]. At the same time, a number of problems impede large-scale applications of SOFCs, among them high-temperature degradation processes, chemical compatibility of cell components and the high cost of materials [1–4]. The lowering of the operating temperature is the general way to promote the commercial application of SOFCs because it broadens the range of compatible construction materials, prolongs their lifetime and, consequently, reduces the cost of energy production. In this respect, proton-conducting solid oxide fuel cells (H-SOFCs) are generally considered to be better suited for practical applications due to lower operating temperatures and the absence of fuel contamination. In turn, conclusions on the chemical compatibility of materials are usually made based only on a costly and time-consuming trial-and-error method: heating a physical mixture of different powders at high temperature for several hours followed by analyzing its phase composition using X-ray diffraction (XRD). Such an approach may lead to contradictory results because of the kinetic limitations of solid-state interaction and non-zero detection limits of conventional XRD. In this respect, thermodynamic analysis of materials' compatibility is completely free from such limitations and, probably, represents the only way of unambiguous interpretation of compounds' stability under particular conditions.

The choice of thermodynamically stable and chemically compatible materials is a necessary but not sufficient condition for successful operation of SOFCs, because solid-state materials exposed to a thermodynamic potential gradient (gradient of temperature,

chemical potential of elements, electrical potential) are subjected to kinetic degradation governed by diffusion processes [5]. The applied gradients induce directed fluxes of the mobile components and lead to three basic degradation phenomena of materials: (i) kinetic demixing, (ii) kinetic decomposition and (iii) morphological instability [5]. Thus, in SOFCs the different chemical natures of components and high operating temperatures (600–1000 °C) inevitably lead to cation interdiffusion and continuous kinetic degradation of materials and, therefore, determine the lifetime of the devices [4].

Obviously, understanding the diffusion processes at the electrode/electrolyte interfaces in SOFCs is of critical importance for their successful large-scale commercial application [4]. Unfortunately, this important information is mostly lacking, and only a limited number of studies of cation diffusion phenomena in perovskite oxides may be found in the literature. Thus, Ca- and Sr-doped $LaCrO_3$, and Sr- and Mg-doped $LaGaO_3$ were investigated by tracer diffusion method [6–8]. Cation interdiffusion in the systems $LaFeO_3$, $LaCoO_3$, $La_{0.9}Sr_{0.1}NiO_4$, $La_2Ni_{0.8}Cu_{0.2}O_4$ and $La_{27}W_5O_{55.5}$ was studied by diffusion couple method [9–13]. The kinetic demixing process was studied only for $La_{0.5}Sr_{0.5}Fe_{0.5}Co_{0.5}O_{3-\delta}$ and $La_{0.3}Sr_{0.7}CoO_{3-\delta}$ [14,15]. Comprehensive investigation was carried out for $La_2NiO_{4+\delta}$, a Ruddlesden–Popper phase, including determination of the self-diffusion coefficient of Ni^{2+} [16], chemical tracer diffusion [17], interdiffusion coefficients for the *A*- and *B*-site cations [18], as well as kinetic decomposition of La_2NiO_{4+d} under an oxygen chemical potential gradient [19]. As for the interdiffusion between the components of SOFCs, to the best of our knowledge this has been studied only for LSCF | GDC | YSZ interfaces, where Gd-doped ceria (GDC) acts as a buffer layer between the $La_{1-x}Sr_xCo_{1-y}Fe_yO_{3-\delta}$ (LSCF) cathode and yttria-stabilized zirconia (YSZ) electrolyte [20,21]. In turn, for proton-conducting SOFCs, such studies have not yet been performed.

The thermodynamic analysis of the stability of the double perovskite $PrBaCo_2O_{6-\delta}$ under different conditions has recently been carried out by us [22]. As a result, its instability against chemical interaction with CeO_2 was found. The diffusion couple ($PrBaCo_2O_{6-\delta}$(PBC)–SDC) experiment showed interdiffusion of Pr and Sm and chemical interaction between PBC and SDC with the formation of barium cerate as a product, in full agreement with thermodynamic calculations. Both phenomena were shown to affect significantly both thermal expansion and total conductivity of the composite electrodes and lead to higher than expected TECs of the composites. Thus, the potential problems with cation interdiffusion have already been outlined [22]. Formation of barium cerate on the border between PBC and SDC was also shown to cause a significant drop in the composites' total conductivity and should be detrimental for the long-term stability of the SOFC cell. One can expect that formation of $BaCO_3$ due to the chemical reaction of PBC with CO_2 from the ambient air, as predicted by thermodynamic calculations, will lead to lowering of the SOFC's performance as well. The PBC double perovskite was shown to be more suitable as an electrode for proton-conducting solid oxide fuel cells because of its thermodynamic stability against chemical interaction with barium-cerate- and zirconate-based electrolytes [22].

In addition, the influence of the sintering aids such as, for example, widely employed NiO on the electrode–electrolyte compatibility and interdiffusion is completely unknown.

Therefore, the priority aims of the present work were (i) to investigate the chemical compatibility of double perovskite cathodes $RBaCo_2O_{6-\delta}$ (*R* = Gd, Pr) with proton-conducting solid electrolyte $BaZr_{0.8}Y_{0.2}O_{3-\delta}$+NiO (0, 1 wt.%) and (ii) to study interdiffusion processes at the interfaces $RBaCo_2O_{6-\delta}$ (*R* = Gd, Pr) | $BaZr_{0.8}Y_{0.2}O_{3-\delta}$+NiO (0, 1 wt.%).

2. Experimental Procedure

Powder samples of the double perovskites $PrBaCo_2O_{6-\delta}$ (PBC) and $GdBaCo_2O_{6-\delta}$ (GBC) and the solid electrolyte $BaZr_{0.8}Y_{0.2}O_{3-\delta}$ (BZY0.2) were prepared by means of a glycerol–nitrate method using Gd_2O_3, Pr_6O_{11}, Y_2O_3, $BaCO_3$, Co and $Zr(OH)_2CO_3{\cdot}xH_2O$ as starting materials. The purity of all the materials used was 99.99% (wt.).

$Zr(OH)_2CO_3 \cdot xH_2O$ was preliminarily dissolved in concentrated HNO_3 (purity 99.99%), and the Zr concentration in the resulting solution was determined by the gravimetric method. The as-obtained solution with known concentration of Zr was used as a precursor for the solid electrolyte synthesis.

For preparation of $BaZr_{0.8}Y_{0.2}O_{3-\delta}$, the stoichiometric quantities of $BaCO_3$ and Y_2O_3 were dissolved in concentrated HNO_3. This solution was mixed with the $Zr(OH)_2CO_3 \cdot xH_2O$ solution described above, and a stoichiometric amount of glycerol (99% purity) was added as a complexing agent and a fuel. The required weight of glycerol was calculated according to full reduction of the nitrates to molecular N_2. The as-obtained solution was heated continuously at 100 °C till complete water evaporation and pyrolysis of the dried precursor. The resulting ash was subsequently calcined at 1100 °C for 24 h in air and then pressed into pellets (10 mm in diameter at 150 MPa) and sintered at 1550 °C for 12 h in air. A composite material of $BaZr_{0.8}Y_{0.2}O_{3-\delta}$ with 1 wt.% of NiO as a sintering aid was made by physical mixing of the components in an agate mortar in an ethanol medium.

For synthesis of the $RBaCo_2O_{6-\delta}$ (R = Gd, Pr) powders, a stoichiometric mixture of the appropriate starting materials was dissolved in concentrated HNO_3, and glycerol (99% purity) was added to the solution. The weight of glycerol was calculated as described above in the case of $BaZr_{0.8}Y_{0.2}O_{3-\delta}$. As-prepared solutions were heated continuously at 100 °C till complete water evaporation and pyrolysis of the dried precursor. To yield the $RBaCo_2O_{6-\delta}$ (R = Gd, Pr) powders, the product of pyrolysis was subsequently calcined at 900, 1000 and 1100 °C for 12 h in air followed by thorough regrinding in an ethanol medium in an agate mortar after each annealing step.

The phase composition of the as-synthesized samples was studied by means of X-ray diffraction (XRD) with an XRD 7000 diffractometer (Shimadzu, Kyoto, Japan) using Cu Kα radiation (λ = 1.5418 Å). The phase identification was performed using the PDF–2 2021 database [23] and Match! software [24]. The XRD patterns demonstrating phase purity of all the as-prepared oxides are presented in Figure S1.

The refinement of the lattice parameters was performed using the Le Bail method as implemented in Rietica 4.0 software [25]. The refined unit cell parameters of the starting double perovskite and electrolyte powders are given in Table S1.

The chemical compatibility of $RBaCo_2O_{6-\delta}$ (R = Gd, Pr) and $BaZr_{0.8}Y_{0.2}O_{3-\delta}$ was studied by annealing the corresponding powder mixtures (50:50 wt.%) at different temperatures in the range 1100–1250 °C for 12 h in air with subsequent phase identification by the XRD.

Ceramic pellets (Ø10 mm × 3 mm) for cation interdiffusion experiments were prepared by dry pressing at 150 MPa and sintering for 12 h in air at 1240, 1250 and 1550 °C for $PrBaCo_2O_{6-\delta}$, $GdBaCo_2O_{6-\delta}$ and $BaZr_{0.8}Y_{0.2}O_{3-\delta}$+NiO (0, 1 wt.%), respectively. Density of the ceramic samples was estimated by the Archimedes method using water as a medium. The relative densities of the as-prepared pellets were 95% for $GdBaCo_2O_{6-\delta}$, 97% for $PrBaCo_2O_{6-\delta}$, 92% for $BaZr_{0.8}Y_{0.2}O_{3-\delta}$ and 95% for $BaZr_{0.8}Y_{0.2}O_{3-\delta}$+NiO (1 wt.%). One surface of each pellet was polished down to 1 μm using diamond suspension. Then it was purified ultrasonically by means of an IL 10 ultrasonic generator (INLAB, Saint Petersburg, Russia) in an ethanol medium and dried at 70 °C in a drying oven in air atmosphere.

Cation interdiffusion was studied by the diffusion couple method. The following diffusion couples were studied: $GdBaCo_2O_{6-\delta}$–$BaZr_{0.8}Y_{0.2}O_{3-\delta}$, $GdBaCo_2O_{6-\delta}$–$BaZr_{0.8}Y_{0.2}O_{3-\delta}$+NiO (1 wt.%), $PrBaCo_2O_{6-\delta}$–$BaZr_{0.8}Y_{0.2}O_{3-\delta}$ and $PrBaCo_2O_{6-\delta}$–$BaZr_{0.8}Y_{0.2}O_{3-\delta}$+NiO (1 wt.%). Before annealing, each diffusion couple was pressed in a special device and fixed with a clamping mechanism. For each system, two independent experiments were performed, both at 1100 °C for 20 h and at 1200 °C for 48 h in air. After annealing, diffusion couples were placed in a silicon form, fixed with epoxy resin and cut perpendicular to the reaction interface. Then cross section of the reaction zone was polished down to 1 μm using diamond suspension, purified ultrasonically in distilled water and dried at 70 °C in a drying oven in air atmosphere. The microstructure and element distribution across the couples' sections were examined by means of scanning electron microscopy (SEM) using a VEGA

3 microscope (Tescan, Brno, Czech Republic) equipped with an Ultim Max 40 (Oxford Instruments, Abingdon, UK) detector for energy dispersive X-ray spectroscopy (EDX).

Additionally, diffusion couples with porous layers of RBaCo$_2$O$_{6-\delta}$ (R = Gd, Pr) on top of the dense ceramic pellet of BaZr$_{0.8}$Y$_{0.2}$O$_{3-\delta}$ were studied to mimic the behavior of SOFCs' cathodes. These diffusion couples were prepared by screen-printing the cathode paste on the polished surface of the ceramic electrolyte pellet. The cathode paste was obtained by thoroughly mixing the powder of double perovskite cobaltite with a solution of polyvinyl butyral (5 wt.%) in ethanol. The as-prepared diffusion couple was annealed at 1100 °C for 6 h in air. The treatment of the reaction zone and subsequent investigation by SEM were performed as described above for the other diffusion couples.

3. Results and Discussion

3.1. Chemical Compatibility

The results of chemical compatibility experiments are shown in Figures 1 and S2. At a first glance, XRD patterns of the sample mixtures look very similar, at least, at temperatures lower than 1100 °C. Such XRD patterns can be readily found in the current literature along with a typical conclusion that they indicate the absence of chemical interaction between the components of the mixture investigated. However, the XRD pattern of the GdBaCo$_2$O$_{6-\delta}$ + BaZr$_{0.8}$Y$_{0.2}$O$_{3-\delta}$ mixture calcined at the highest studied temperature (see Figure 1) clearly indicates the formation of a new compound isostructural to Gd$_2$O$_3$ (possibly doped by Y$_2$O$_3$). Furthermore, the intensities of the peaks corresponding to the components of the mixtures as well as peaks' positions (and, hence, lattice parameters) depend on the calcination temperature as seen in Figure 1c,d. For example, the intensities of the peaks corresponding to double perovskites RBaCo$_2$O$_{6-\delta}$ (R = Gd, Pr) strongly decrease with calcination temperature. At the same time, XRD peaks of BaZr$_{0.8}$Y$_{0.2}$O$_{3-\delta}$ slightly increase in intensity and shift towards high 2Θ° angles. Similar changes can be observed in the XRD patterns of the mixtures containing NiO; see Figure S2. All these evidences undoubtedly indicate in favor of chemical interaction between double perovskites and a solid electrolyte which occurs already at 1100 °C and likely at lower temperatures. The XRD results seem to suggest at least partial dissolution of RBaCo$_2$O$_{6-\delta}$ (R = Gd, Pr) in BaZr$_{0.8}$Y$_{0.2}$O$_{3-\delta}$ oxide. Therefore, the similarity of the XRD patterns of the starting mixture (denoted as 25 °C in Figure 1) and the one calcined at 1100 °C cannot be used as evidence of the absence of chemical interaction.

The refined unit cell parameters of RBaCo$_2$O$_{6-\delta}$ (R = Gd, Pr) and BaZr$_{0.8}$Y$_{0.2}$O$_{3-\delta}$ after annealing the powder mixtures (50:50 wt.%) are shown in Figure 2.

As seen in Figure 2a,b, lattice parameters of RBaCo$_2$O$_{6-\delta}$ (R = Gd, Pr) oxides, first slightly increase but then decrease with increasing calcination temperature. This can be explained by the combined effect of two factors: (i) variation of the RBaCo$_2$O$_{6-\delta}$ oxygen content, 6−δ, in a wide range [26,27] with temperature and the sample's prehistory and (ii) partial substitution of the smaller Y^{3+} cation for larger Gd^{3+} and Pr^{3+} [28] in RBaCo$_2$O$_{6-\delta}$ due to cation interdiffusion between components of the sample mixture.

As for BaZr$_{0.8}$Y$_{0.2}$O$_{3-\delta}$, its unit cell parameter, as seen in Figure 2c, decreases with calcination temperature and more strongly in contact with GdBaCo$_2$O$_{6-\delta}$ oxide. This can be, at least qualitatively, explained assuming cobalt dissolution in BaZr$_{0.8}$Y$_{0.2}$O$_{3-\delta}$ leads to lattice contraction as shown in [29], whereas dissolution of Gd and Pr, on the contrary, facilitates the lattice expansion of barium zirconate due to differences in the cation radii [28].

3.2. Analysis of Diffusion Couples

The results of SEM and EDX analysis of the cross sections of diffusion couples RBaCo$_2$O$_{6-\delta}$ (R = Gd, Pr)–BaZr$_{0.8}$Y$_{0.2}$O$_{3-\delta}$+NiO (0, 1 wt.%) after annealing are presented in Figures 3–5. They support the conclusions drawn above and based on the results of chemical compatibility study by XRD. As seen in Figures 3–5, cation interdiffusion can be observed, with Co being the most mobile cation demonstrating pronounced diffusion into the electrolyte pellet for all the couples studied.

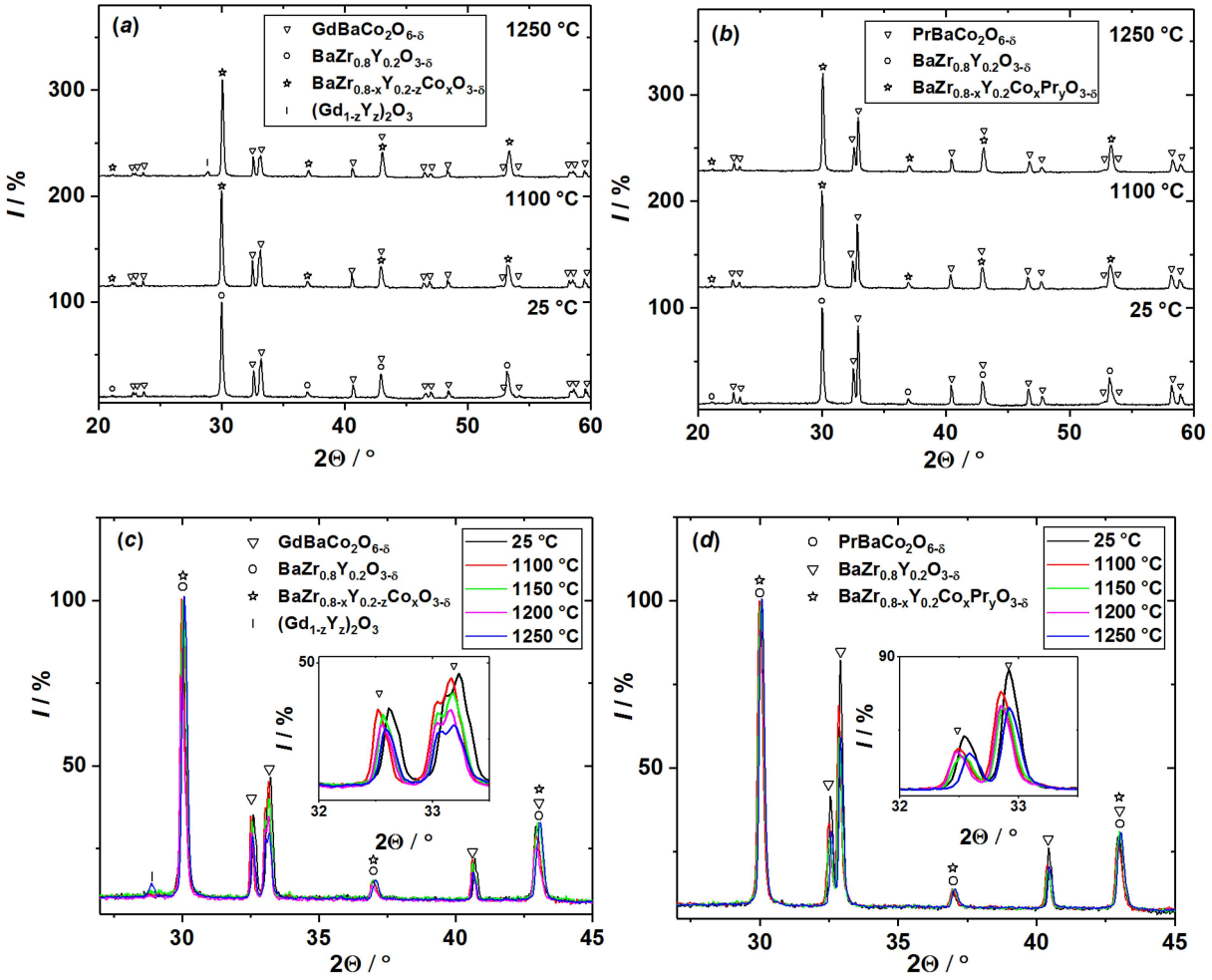

Figure 1. XRD patterns of the powder mixtures RBaCo$_2$O$_{6-\delta}$–BaZr$_{0.8}$Y$_{0.2}$O$_{3-\delta}$ (50:50 wt.%) annealed at different temperatures for 12 h in air: (**a**,**c**) R = Gd; (**b**,**d**) R = Pr.

The analysis of the cross section of the GdBaCo$_2$O$_{6-\delta}$–BaZr$_{0.8}$Y$_{0.2}$O$_{3-\delta}$ diffusion couple annealed at 1200 °C for 48 h in air, as seen in Figure 3a, reveals the formation of Gd$_2$O$_3$ on the surface of the GdBaCo$_2$O$_{6-\delta}$ pellet along the interface of the diffusion couple. This is obviously in agreement with the XRD results discussed above. In addition, slight interdiffusion (depth ~15 μm) of Gd^{3+} ions in the BaZr$_{0.8}$Y$_{0.2}$O$_{3-\delta}$ electrolyte and Y^{3+} into the GdBaCo$_2$O$_{6-\delta}$ phase was detected. The diffusion of Co ions occurs mainly through the bulk of the electrolyte. The diffusion depth reaches 300 μm. Cobalt concentration in the electrolyte pellet is practically constant at a distance of up to 30 μm from the interface with GdBaCo$_2$O$_{6-\delta}$. The average chemical composition of this electrolyte layer was estimated as Ba$_{1.02}$Zr$_{0.76}$Y$_{0.16}$Co$_{0.06}$O$_{3-\delta}$.

In the case of the PrBaCo$_2$O$_{6-\delta}$–BaZr$_{0.8}$Y$_{0.2}$O$_{3-\delta}$ couple annealed at 1200 °C for 48 h in air, significant diffusion of both Co and Pr into the BaZr$_{0.8}$Y$_{0.2}$O$_{3-\delta}$ pellet was found, as shown in Figure 4a. Their diffusion occurs both along the grain boundaries and through the bulk of BaZr$_{0.8}$Y$_{0.2}$O$_{3-\delta}$. The former mechanism is dominating. The diffusion depth of Co reaches 560 μm. The analysis of the grain boundary phase's chemical composition gives near the interface PrBaCo$_2$O$_{6-\delta}$ | BaZr$_{0.8}$Y$_{0.2}$O$_{3-\delta}$ the following averaged composition: Ba$_{1.02}$Co$_{0.72}$Y$_{0.21}$Pr$_{0.09}$O$_{3-\delta}$. However, the composition of the grains' interior may be expressed as Ba$_{0.99}$Zr$_{0.69}$Y$_{0.16}$Co$_{0.13}$Pr$_{0.03}$O$_{3-\delta}$.

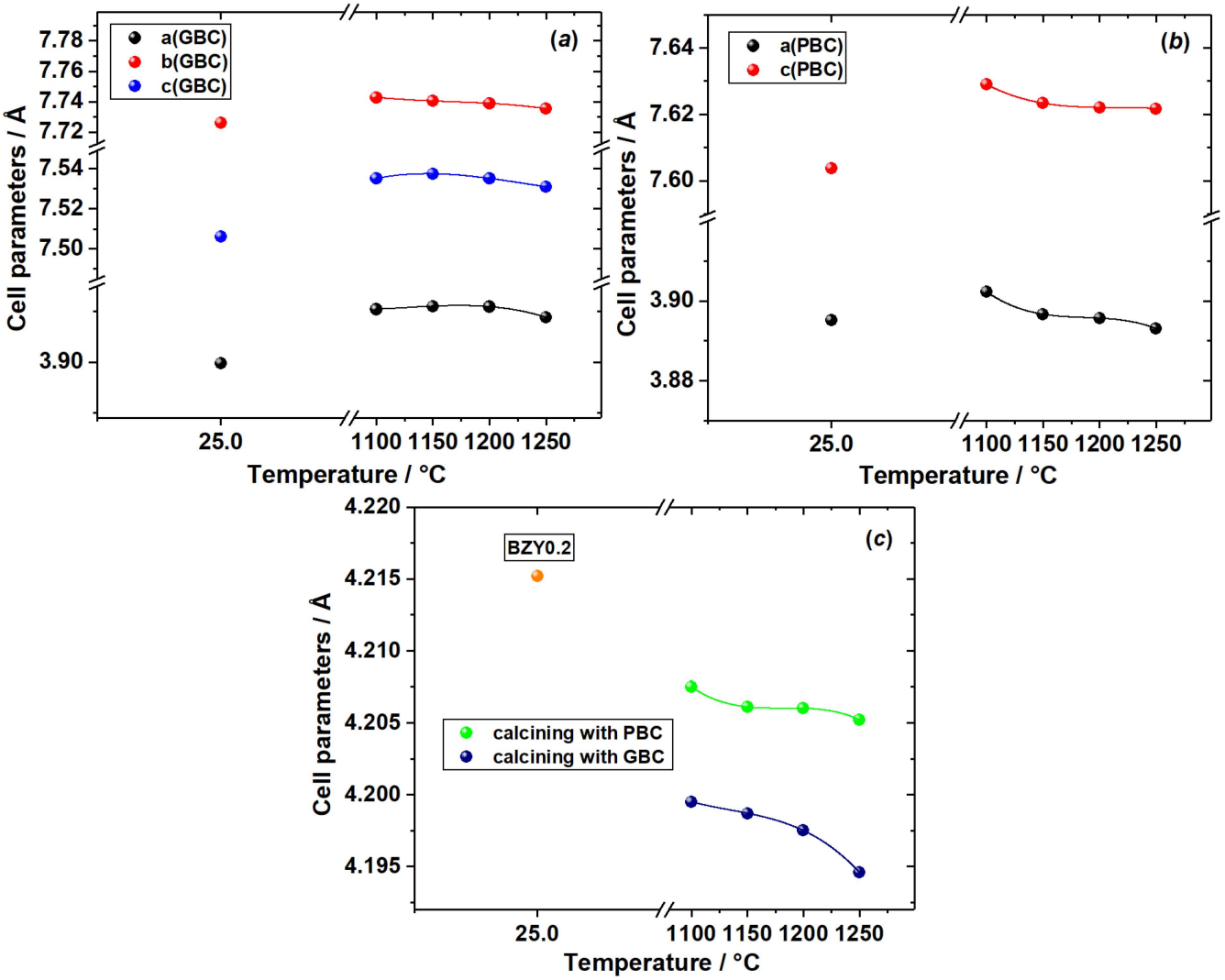

Figure 2. The unit cell parameters vs. annealing temperature of powder mixtures RBaCo$_2$O$_{6-\delta}$ (R = Gd, Pr)–BaZr$_{0.8}$Y$_{0.2}$O$_{3-\delta}$ (50:50 wt.%): (**a**) GdBaCo$_2$O$_{6-\delta}$, (**b**) PrBaCo$_2$O$_{6-\delta}$ and (**c**) BaZr$_{0.8}$Y$_{0.2}$O$_{3-\delta}$.

The addition of NiO as a sintering aid to the BaZr$_{0.8}$Y$_{0.2}$O$_{3-\delta}$ solid electrolyte strongly promotes interdiffusion especially along the grain boundaries, as can be observed in Figures 3b, 4b and S3. As a result, for example, the depth of Co diffusion from PrBaCo$_2$O$_{6-\delta}$ to BaZr$_{0.8}$Y$_{0.2}$O$_{3-\delta}$ is almost doubled, up to 1000 μm when 1 wt.% of NiO is added to the electrolyte.

The diffusion couple GdBaCo$_2$O$_{6-\delta}$–BaZr$_{0.8}$Y$_{0.2}$O$_{3-\delta}$+NiO (1 wt.%) annealed at 1200 °C for 48 h in air does not show the formation of Gd_2O_3 as a reaction product, contrary to the couple without NiO. Instead, diffusion of Gd^{3+} into the electrolyte phase occurs mainly through the grain boundary mechanism, as seen in Figure 3b. Similar behavior is evident for diffusion of Co ions. As a result, the formation of Ba$_{1.03}$Co$_{0.81}$Ni$_{0.03}$Gd$_{0.13}$O$_{3-\delta}$ oxide was detected on the grain boundaries of the electrolyte pellet near the interface with double perovskite, whereas the composition of the electrolyte grains' bulk corresponds to Ba$_{1.02}$Zr$_{0.78}$Y$_{0.16}$Co$_{0.04}$O$_{3-\delta}$. In addition, the diffusion of Ni^{2+} ions from the electrolyte pellet to the GdBaCo$_2$O$_{6-\delta}$ phase was observed.

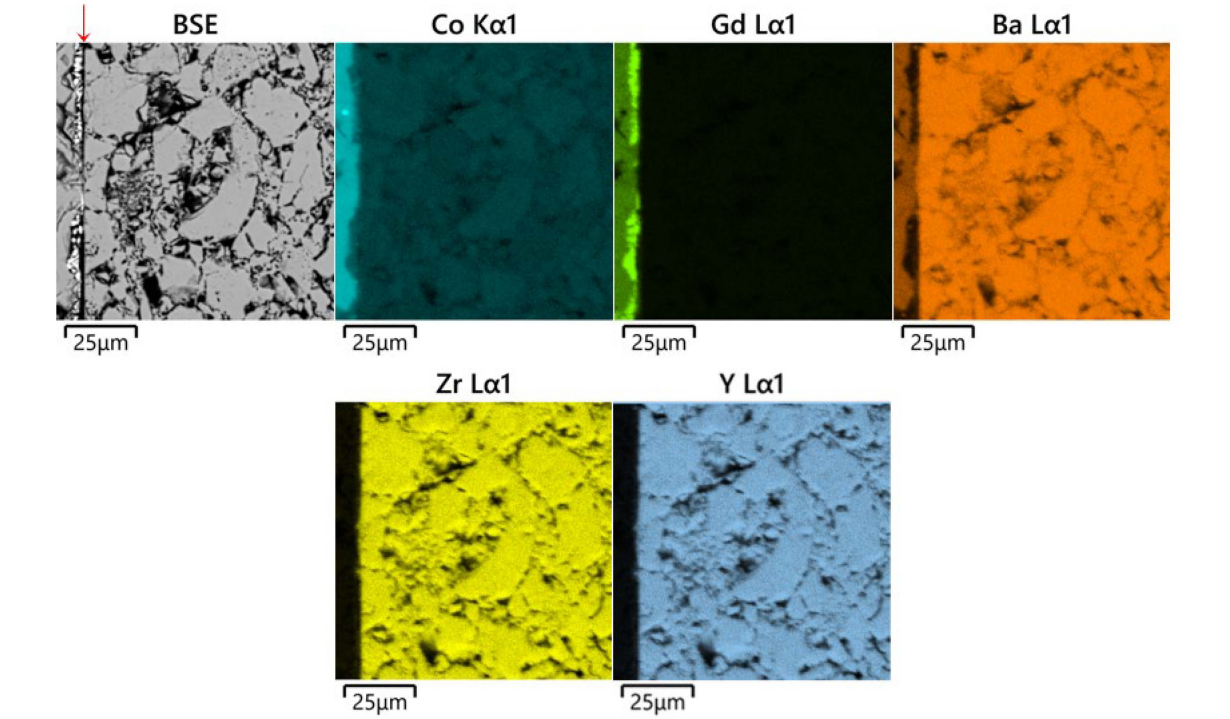

(**a**)

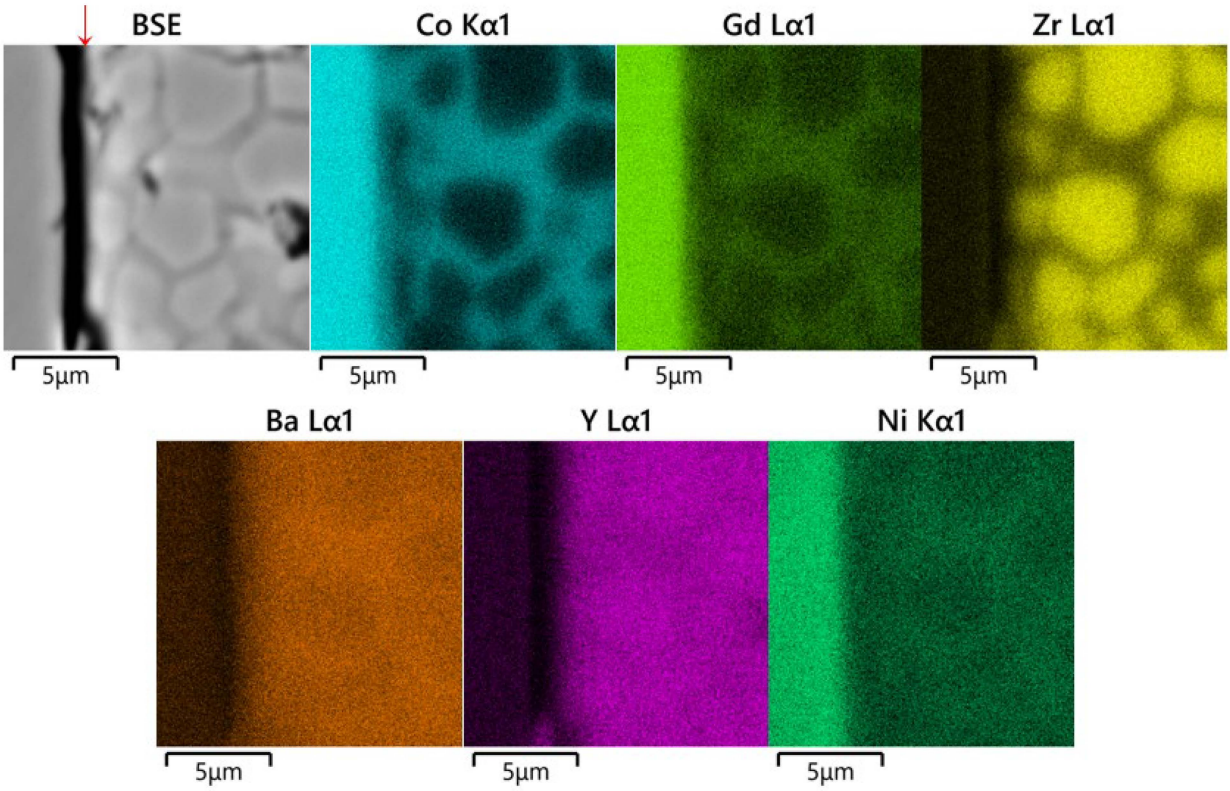

(**b**)

Figure 3. SEM images and concentration maps of reaction zones for diffusion couples after annealing at 1200 °C for 48 h in air: (**a**) $GdBaCo_2O_{6-\delta}$–$BaZr_{0.8}Y_{0.2}O_{3-\delta}$ and (**b**) $GdBaCo_2O_{6-\delta}$–$BaZr_{0.8}Y_{0.2}O_{3-\delta}$+NiO (1 wt.%); BSE (back scattered electrons) image and element maps were obtained near the phase boundary of the diffusion couple. The red arrow marks the interface between the pellets.

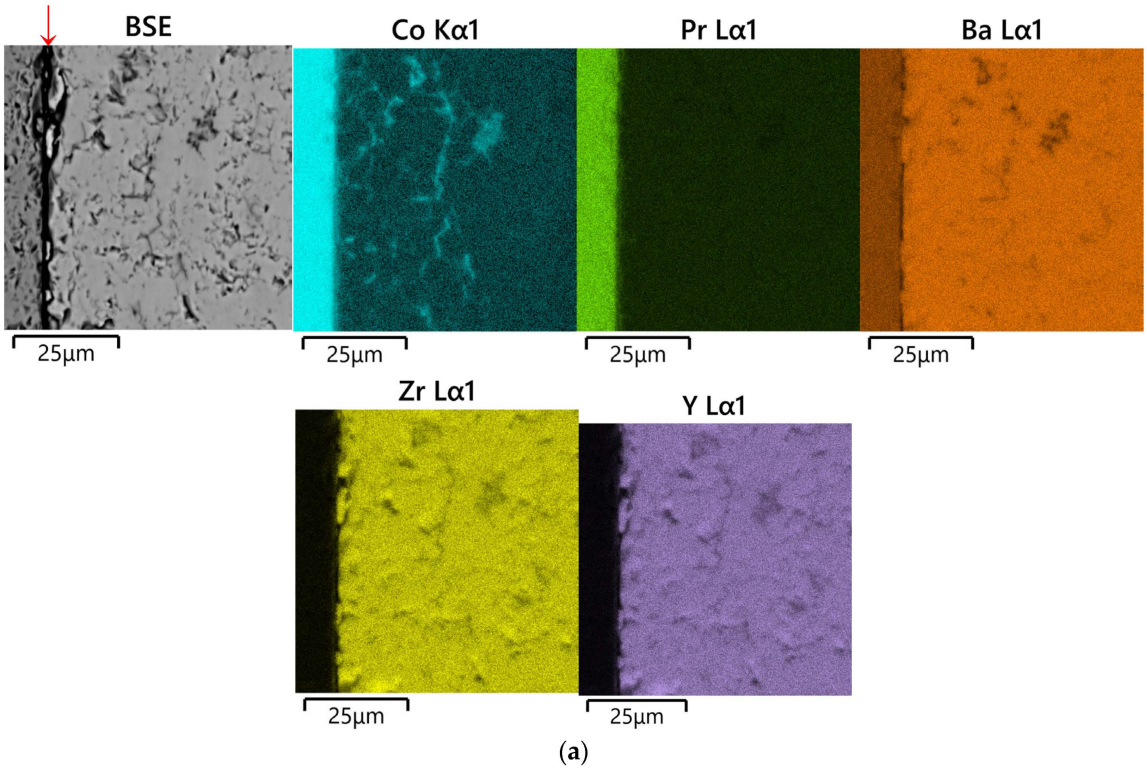

(**a**)

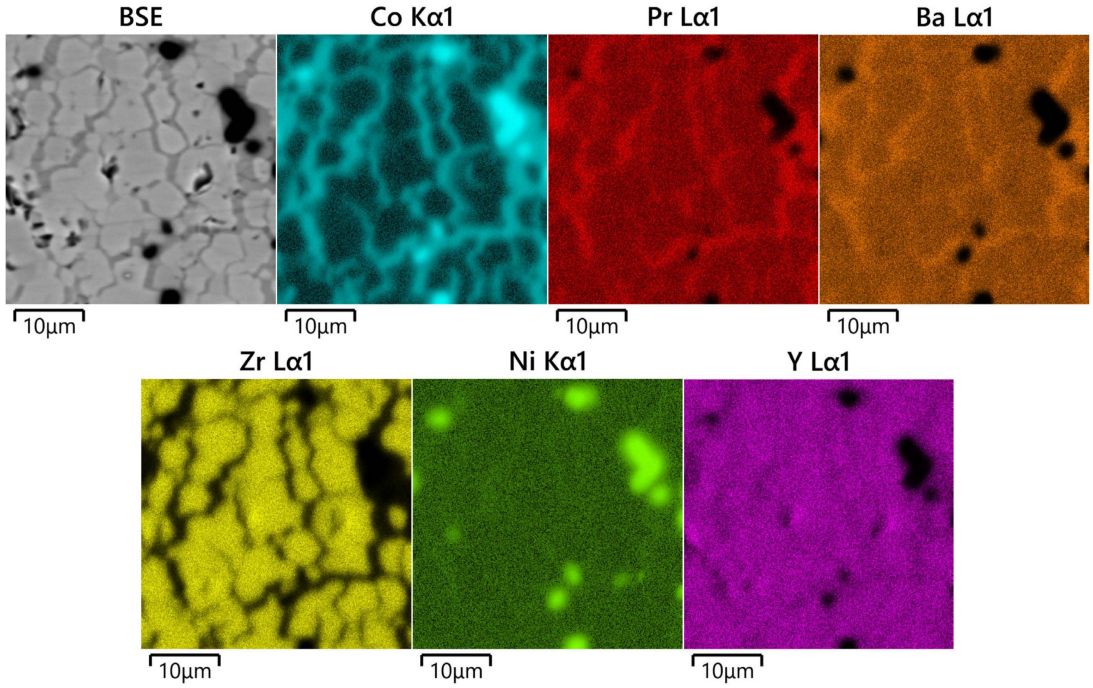

(**b**)

Figure 4. SEM images and concentration maps of reaction zones for diffusion couples after annealing at 1200 °C for 48 h in air: (**a**) $PrBaCo_2O_{6-\delta}$–$BaZr_{0.8}Y_{0.2}O_{3-\delta}$; BSE image and element maps obtained near the phase boundary of diffusion couple and (**b**) $PrBaCo_2O_{6-\delta}$–$BaZr_{0.8}Y_{0.2}O_{3-\delta}$+NiO (1 wt.%); BSE image and element maps obtained in the area of Co diffusion maximum in the depth of about 500 μm from the phase boundary. The corresponding images near the phase boundary of the diffusion couple may be observed in Figure S3. The red arrow marks the interface between the pellets.

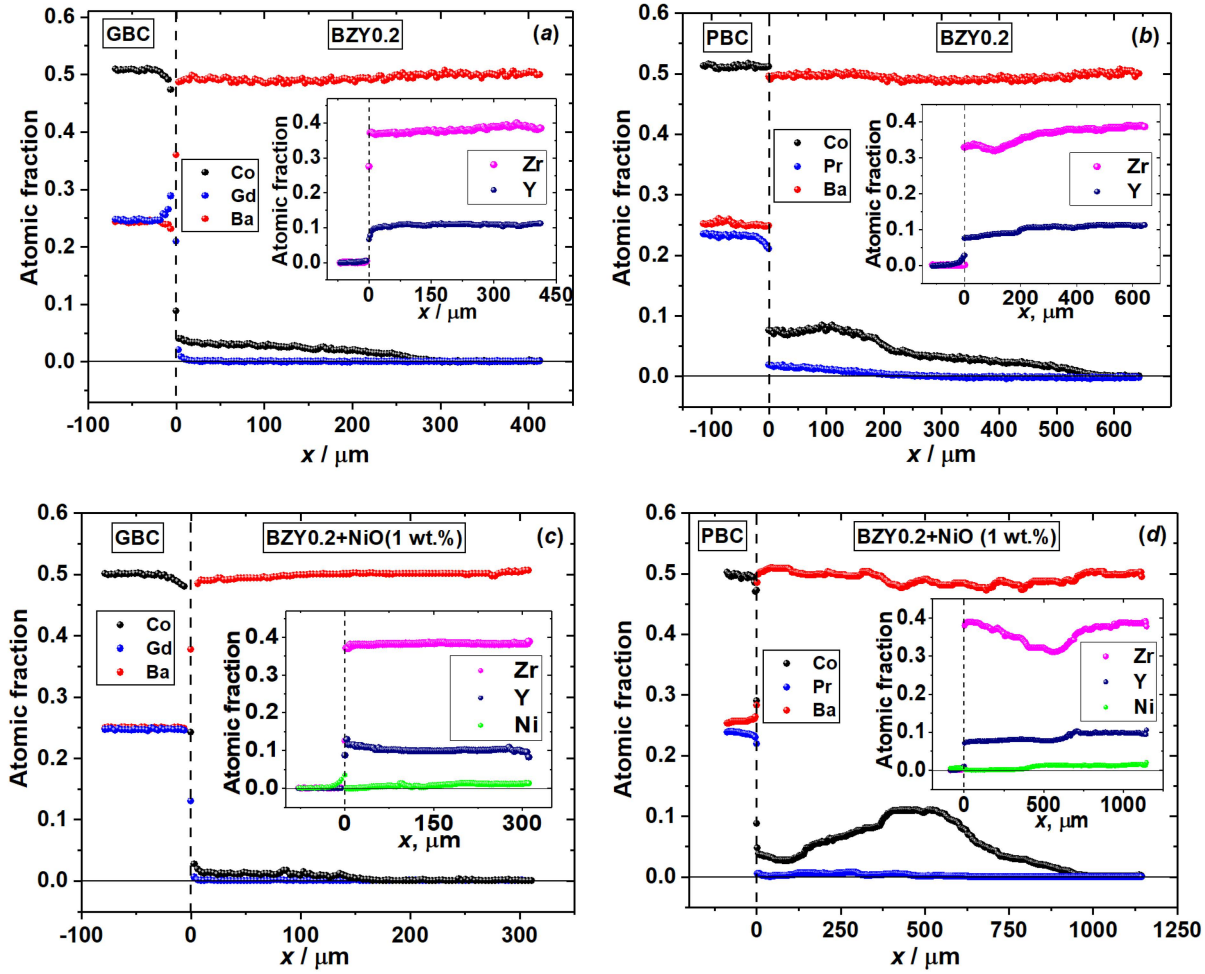

Figure 5. Concentration profiles of diffusion couples after annealing at 1200 °C for 48 h in air: (**a**) $GdBaCo_2O_{6-\delta}$–$BaZr_{0.8}Y_{0.2}O_{3-\delta}$, (**b**) $PrBaCo_2O_{6-\delta}$–$BaZr_{0.8}Y_{0.2}O_{3-\delta}$, (**c**) $GdBaCo_2O_{6-\delta}$–$BaZr_{0.8}Y_{0.2}O_{3-\delta}$+NiO (1 wt.%) and (**d**) $PrBaCo_2O_{6-\delta}$–$BaZr_{0.8}Y_{0.2}O_{3-\delta}$+NiO (1 wt.%).

The largest diffusion depth, reaching 1000 μm, was found in the $PrBaCo_2O_{6-\delta}$–$BaZr_{0.8}Y_{0.2}O_{3-\delta}$+NiO (1 wt.%) couple annealed at 1200 °C for 48 h in air. Again, the diffusion of Pr and Co occurs through both grain boundaries and bulk of the electrolyte phase with the former mechanism being the dominating one. Interestingly, it seems in this case the cation diffusion in the electrolyte pellet so strongly depends on the presence of NiO that near the interface, where the concentration of Ni is relatively lower than that in the bulk of the electrolyte pellet due to nickel diffusion into the double perovskite pellet, a layer depleted in Co and Pr is formed. The maximum of Co concentration is, thus, shifted deep into the electrolyte pellet at a distance of 400–540 μm from the interface with double perovskite. In this area, two types of Co-containing compounds were observed. The one with an approximate composition $Y_{0.70}Pr_{0.24}Ba_{0.94}Co_{1.76}Ni_{0.12}O_{6-\delta}$ was detected on the grain boundaries (Figure 4b). The other is a mixed cobalt–nickel oxide with Co to Ni ratio 2.04:0.9, which forms particles with a size of about 2–5 μm, as seen in Figure 4b. The composition of the bulk of the electrolyte's grains in the area of maximum cobalt content corresponds on average to $Ba_{1.01}Zr_{0.80}Y_{0.16}Co_{0.03}O_{3-\delta}$.

The averaged (over the cross section area) concentration profiles illustrating the above-mentioned distribution of different species in the diffusion zone of the $RBaCo_2O_{6-\delta}$ (R = Gd, Pr) | $BaZr_{0.8}Y_{0.2}O_{3-\delta}$+NiO (0, 1 wt.%) couples annealed at 1200 °C for 48 h in air are shown in Figure 5.

Decreasing the annealing temperature of all the diffusion couples discussed above to 1100 °C does not change the general view of the diffusion zone except that the diffusion depth roughly becomes two times less than that at 1200 °C. In the case of porous RBaCo$_2$O$_{6-\delta}$ (R = Gd, Pr) double perovskite layers annealed on the surface of the pure BaZr$_{0.8}$Y$_{0.2}$O$_{3-\delta}$ electrolyte pellet at 1100 °C for 6 h in air, i.e., under conditions which can be used to produce a cathode layer in the SOFC, the diffusion depth was found to be equal to ~50 μm irrespective of the nature of rare-earth element. Taking into account the typical thickness of the electrolyte layer of the order of 10–50 μm, the results of this work give a clear indication that for the time necessary for the preparation of the cathode layer, cobalt from the double perovskite seems to be able to reach the SOFC's anode, diffusing through the electrolyte layer. Since the leading diffusion mechanism is the grain boundary one, all the electrolyte grains in that case would be covered with Co-rich compounds. This would potentially lead to electrolyte breakage due to cobalt cations' reduction by hydrogen from the anode compartment. Hence, the cation interdiffusion puts strong technological restrictions on the use of cobaltites in proton-conducting SOFCs with BaZr$_{1-x}$Y$_x$O$_{3-\delta}$-based electrolytes. Methods must be found to prevent or at least reduce the diffusion of cobalt into the electrolyte by, for example, using some buffer layer; alternatively, other cathode materials that are less prone to similar diffusion problems should be identified.

In any case, the results of our work convincingly point to the crucial necessity of performing similar studies with other potential cathode and electrolyte materials of proton-conducting SOFCs. Furthermore, the NiO-sintering aid, as discussed above, seems to promote the grain boundary diffusion in the electrolyte layer, hence, the quantity of NiO should be limited and the influence of other sintering aids on diffusion in the system electrode | electrolyte should be studied.

4. Conclusions

Chemical compatibility and cation interdiffusion between the double perovskites RBaCo$_2$O$_{6-\delta}$ (R = Gd, Pr) and proton-conducting electrolyte BaZr$_{0.8}$Y$_{0.2}$O$_{3-\delta}$ were studied by XRD and diffusion couples methods. Both techniques gave consistent results indicating that chemical interaction between the double perovskites and the solid electrolyte occurs already at 1100 °C and, likely, at lower temperatures. The partial dissolution of RBaCo$_2$O$_{6-\delta}$ (R = Gd, Pr) in BaZr$_{0.8}$Y$_{0.2}$O$_{3-\delta}$ oxide was found. Element distribution maps obtained through the cross sections of diffusion couples showed strong interdiffusion of cations, with cobalt being the most mobile cation possessing in some instances the diffusion depth in the electrolyte up to several hundreds of micrometers. In the case of the GdBaCo$_2$O$_{6-\delta}$ | BaZr$_{0.8}$Y$_{0.2}$O$_{3-\delta}$ couple without the NiO-sintering aid, Co diffusion occurs through the bulk of the electrolyte phase, whereas a layer of Gd$_2$O$_3$ forms on the interface with double perovskite. Yet, in the presence of NiO, both Gd and Co diffuse from GdBaCo$_2$O$_{6-\delta}$ inside the electrolyte pellet with the grain boundary mechanism as the main one. In turn, when PrBaCo$_2$O$_{6-\delta}$ is in contact with BaZr$_{0.8}$Y$_{0.2}$O$_{3-\delta}$, the diffusion of both Pr and Co in the electrolyte pellet takes place irrespective of NiO addition. The diffusion occurs through both bulk and grain boundary mechanisms, with the latter as the leading one. The diffusion depth in the presence of the NiO-sintering aid is almost doubled, pointing to the necessity to control the content of NiO in the electrolyte as well as to search for other sintering aids. The observed strong diffusion of cobalt through the BaZr$_{0.8}$Y$_{0.2}$O$_{3-\delta}$ layer reveals a potential problem for the long-term stability of SOFCs and, thus, must be understood and controlled as much as possible.

Supplementary Materials: The following supporting information can be downloaded at: https://www.mdpi.com/article/10.3390/en16072980/s1. Figure S1. XRD patterns of the as-prepared oxides: (a) GdBaCo$_2$O$_{6-\delta}$, (b) PrBaCo$_2$O$_{6-\delta}$, (c) BaZr$_{0.8}$Y$_{0.2}$O$_{3-\delta}$; Table S1. Refined unit cell parameters of the as-prepared oxides; Figure S2. XRD patterns of the powder mixtures (50:50 wt.%) RBaCo$_2$O$_{6-\delta}$–BaZr$_{0.8}$Y$_{0.2}$O$_{3-\delta}$ +NiO (1 wt.%) annealed at different temperatures for 12 h in air: (a) R = Gd, (b) R = Pr; Figure S3. BSE image and concentration maps near the phase boundary of the

$PrBaCo_2O_{6-\delta}$–$BaZr_{0.8}Y_{0.2}O_{3-\delta}$+NiO (1 wt.%) diffusion couple after annealing at 1200 °C for 48 h in air.

Author Contributions: Conceptualization, N.S.T. and D.S.T.; methodology, N.S.T. and D.S.T.; validation, A.Y.Z. and I.L.I.; formal analysis, N.S.T., D.S.T., A.Y.Z. and D.A.M.; investigation, N.S.T., D.A.M. and I.L.I.; writing—original draft preparation, N.S.T., D.S.T. and A.Y.Z.; writing—review and editing, N.S.T., D.S.T., I.L.I., D.A.M. and A.Y.Z. All authors have read and agreed to the published version of the manuscript.

Funding: This work was supported by the Ministry of Science and Higher Education of the Russian Federation (State Assignment № No. 075-03-2021-051/5).

Data Availability Statement: The reported data are available by reasonable request from the corresponding authors.

Conflicts of Interest: The authors declare no conflict of interest.

References

1. Boudghene Stambouli, A.; Traversa, E. Solid oxide fuel cells (SOFCs): A review of an environmentally clean and efficient source of energy. *Renew. Sustain. Energy Rev.* **2002**, *6*, 433–455. [CrossRef]
2. Mahato, N.; Banerjee, A.; Gupta, A.; Omar, S.; Balani, K. Progress in material selection for solid oxide fuel cell technology: A review. *Prog. Mater. Sci.* **2015**, *72*, 141–337. [CrossRef]
3. Kumar, R.V.; Khandale, A.P. A review on recent progress and selection of cobalt-based materials for low temperature-solid oxide fuel cells. *Renew. Sustain. Energy Rev.* **2022**, *156*, 111985. [CrossRef]
4. Khan, M.Z.; Song, R.-H.; Mehran, M.T.; Lee, S.-B.; Lim, T.-H. Controlling cation migration and inter-diffusion across cathode/interlayer/electrolyte interfaces of solid oxide fuel cells: A review. *Ceram. Int.* **2021**, *47*, 5839–5869. [CrossRef]
5. Martin, M. Materials in thermodynamic potential gradients. *J. Chem. Thermodyn.* **2003**, *35*, 1291–1308. [CrossRef]
6. Sakai, N.; Yamaji, K.; Horita, T.; Negishi, H.; Yokokawa, H. Chromium diffusion in lanthanum chromites. *Solid State Ion.* **2000**, *135*, 469–474. [CrossRef]
7. Horita, T.; Ishikawa, M.; Yamaji, K.; Sakai, N.; Yokokawa, H.; Dokiya, M. Calcium tracer diffusion in (La,Ca)CrO_3 by SIMS. *Solid State Ion.* **1999**, *124*, 301–307. [CrossRef]
8. Shulz, O.; Martin, M.; Argirusis, C.; Borchardt, G. Cation tracer diffusion of ^{138}La, ^{84}Sr and ^{25}Mg in polycrystalline $La_{0.9}Sr_{0.1}Ga_{0.9}Mg_{0.1}O_{2.9}$. *Phys. Chem. Chem. Phys.* **2003**, *5*, 2308–2313. [CrossRef]
9. Smith, J.B.; Norby, T. Cation self-diffusion in $LaFeO_3$ measured by the solid state reaction. *Solid State Ion.* **2006**, *177*, 639–646. [CrossRef]
10. Smith, J.B.; Norby, T. Electron probe micro analysis of A-site inter-diffusion between $LaFeO_3$ and $NdFeO_3$. *J. Am. Ceram. Soc.* **2006**, *89*, 582–586. [CrossRef]
11. Palcut, M.; Wiik, K.; Grande, T. cation self-diffusion in $LaCoO_3$ and La_2CoO_4 studied by diffusion couple experiments. *J. Phys. Chem. B* **2007**, *111*, 2299–2308. [CrossRef]
12. Čebašek, N.; Haugsrud, R.; Norby, T. Cation transport in Sr and Cu substituted $La_2NiO_{4+\delta}$ studied by inter-diffusion. *Solid State Ion.* **2014**, *254*, 32–39. [CrossRef]
13. Vollestad, E.; Norby, T.; Haugsrud, R. Inter-diffusion in lanthanum tungsten oxide. *Solid State Ion.* **2013**, *244*, 57–62. [CrossRef]
14. Lein, H.L.; Wiik, K.; Grande, T. Kinetic demixing and decomposition of oxygen permeable membranes. *Solid State Ion.* **2006**, *177*, 1587–1590. [CrossRef]
15. Doorn van, R.H.E.; Bouwmeester, H.J.M.; Burggraaf, A.J. Kinetic decomposition of $La_{0.3}Sr_{0.7}CoO_{3-\delta}$ perovskite membranes during oxygen permeation. *Solid State Ion.* **1998**, *111*, 263–272. [CrossRef]
16. Čebašek, N.; Haugsrud, R.; Milošević, J.; Li, Z.; Smith, J.B.; Magrasó, A.; Norby, T. Determination of the self-diffusion coefficient of Ni^{2+} in La_2NiO_{4+d} by the solid state reaction method. *J. Electrochem. Soc.* **2012**, *159*, B702–B708. [CrossRef]
17. Čebašek, N.; Haugsrud, R.; Li, Z.; Norby, T. Determination of chemical tracer diffusion coefficient for the La- and Ni-site in La_2NiO_{4+d} studied by SIMS. *J. Am. Ceram. Soc.* **2013**, *96*, 598–605. [CrossRef]
18. Čebašek, N.; Haugsrud, R.; Norby, T. Determination of inter-diffusion coefficient for the A- and B-site in the A_2BO_{4+d} (A = La, Nd and B = Ni, Cu) system. *Solid State Ion.* **2013**, *231*, 74–80. [CrossRef]
19. Čebašek, N.; Norby, T.; Li, Z. Kinetic Decomposition of a La_2NiO_{4+d} membrane under an oxygen potential gradient. *J. Electrochem. Soc.* **2012**, *159*, F461–F467. [CrossRef]
20. Li, Z.-P.; Mori, T.; Auchterlonie, G.J.; Zou, J.; Drennan, J. Two types of diffusions at the cathode/electrolyte interface in It-SOFCs. *J. Solid State Chem.* **2011**, *184*, 2458–2461. [CrossRef]
21. Matsui, T.; Li, S.; Yu, I.; Yoshida, N.; Muroyama, H.; Eguchi, K. Degradation analysis of solid oxide fuel cells with (La,Sr)(Co,Fe)$O_{3-\delta}$ cathode/Gd_2O_3-CeO_2 interlayer/Y_2O_3-ZrO_2 electrolyte system: The influences of microstructural change and solid solution formation. *J. Electrochem. Soc.* **2019**, *166*, F295–F300. [CrossRef]
22. Tsvetkov, D.; Tsvetkova, N.; Ivanov, I.; Malyshkin, D.; Sereda, V.; Zuev, A. $PrBaCo_2O_{6-\delta}$-$Ce_{0.8}Sm_{0.2}O_{1.9}$ Composite Cathodes for Intermediate-Temperature Solid Oxide Fuel Cells: Stability and Cation Interdiffusion. *Energies* **2019**, *12*, 417. [CrossRef]

23. Available online: http://www.icdd.com/products/pdf2.htm (accessed on 30 January 2023).
24. Available online: http://www.crystalimpact.com/match/Default.htm (accessed on 30 January 2023).
25. Hunter, B.A. RIETICA, version 1.7.7. *IUCR Powder Diffr.* **1997**, *22*, 21–26.
26. Tsvetkov, D.S.; Sereda, V.V.; Zuev, A.Y. Oxygen nonstoichiometry and defect structure of the double perovskite $GdBaCo_2O_{6-\delta}$. *Solid State Ion.* **2010**, *180*, 1620–1625. [CrossRef]
27. Tsvetkov, D.S.; Ivanov, I.L.; Malyshkin, D.A.; Zuev, A.Y. Oxygen content, cobalt oxide exsolution and defect structure of the double perovskite $PrBaCo_2O_{6-\delta}$. *J. Mater. Chem. A* **2016**, *4*, 1962–1969. [CrossRef]
28. Shannon, R.D. Revised effective ionic radii and systematic studies of interatomic distances in halides and chalcogenides. *Acta Cryst.* **1976**, *32*, 751–767. [CrossRef]
29. Rao, Y.; Zhong, S.; He, F.; Wang, Z.; Peng, R.; Lu, Y. Cobalt-doped $BaZrO_3$: A single phase air electrode material for reversible solid oxide cells. *Int. J. Hydrog. Energy* **2012**, *37*, 12522–12527. [CrossRef]

Disclaimer/Publisher's Note: The statements, opinions and data contained in all publications are solely those of the individual author(s) and contributor(s) and not of MDPI and/or the editor(s). MDPI and/or the editor(s) disclaim responsibility for any injury to people or property resulting from any ideas, methods, instructions or products referred to in the content.